Received: 25 January 2022 | Revised: 5 May 2022 | Accepted: 9 May 2022 | Published on: 9 June 2022

DOI: 10.1002/mrm.29315

RESEARCH ARTICLE

Magnetic Resonance in Medicine

Modeling the Effect of Hyperoxia on the Spin–Lattice Relaxation Rate R1 of Tissues

Emma Bluemke | **Eleanor Stride** | **Daniel Peter Bulte**

Institute of Biomedical Engineering, Department of Engineering Sciences, University of Oxford, Oxford, UK

Correspondence
Emma Bluemke, Institute of Biomedical Engineering, Old Road Campus Research Building, University of Oxford, Headington, Oxford, Oxfordshire, OX3 7DQ, UK.
Email: emma.bluemke@new.ox.ac.uk

Funding information
Clarendon Scholarship fund, Grant/Award Numbers: EP/S021507/1, EP/L024012/1; Medical Research Council, Grant/Award Number: EP/L016052/1; Engineering and Physical Sciences Research Council

Purpose: Inducing hyperoxia in tissues is common practice in several areas of research, including oxygen-enhanced MRI (OE-MRI), which attempts to use the resulting signal changes to detect regions of tumor hypoxia or pulmonary disease. The linear relationship between PO_2 and R1 has been reproduced in phantom solutions and body fluids such as vitreous fluid; however, in tissue and blood experiments, factors such as changes in deoxyhemoglobin levels can also affect the $\Delta R1$.

Theory and Methods: This manuscript proposes a three-compartment model for estimating the hyperoxia-induced changes in R1 of tissues depending on B0, SO_2, blood volume, hematocrit, oxygen extraction fraction, and changes in blood and tissue PO_2. The model contains two blood compartments (arterial and venous) and a tissue compartment. This model has been designed to be easy for researchers to tailor to their tissue of interest by substituting their preferred model for tissue oxygen diffusion and consumption. A specific application of the model is demonstrated by calculating the resulting $\Delta R1$ expected in healthy, hypoxic and necrotic tumor tissues. In addition, the effect of sex-based hematocrit differences on $\Delta R1$ is assessed.

Results: The $\Delta R1$ values predicted by the model are consistent with reported literature OE-MRI results: with larger positive changes in the vascular periphery than hypoxic and necrotic regions. The observed sex-based differences in $\Delta R1$ agree with findings by Kindvall et al. suggesting that differences in hematocrit levels may sometimes be a confounding factor in $\Delta R1$.

Conclusion: This model can be used to estimate the expected tissue $\Delta R1$ in oxygen-enhanced MRI experiments.

KEYWORDS
hyperoxia, longitudinal relaxation, oxygen, oxygen-enhanced MRI, R1, tissue

1 | INTRODUCTION

Many researchers have investigated using the paramagnetic relaxivity effect of oxygen on longitudinal relaxation rate R1 (1/T1) as a means of inferring oxygenation levels. For example, measurements of R1 have been used to infer oxygen levels in vitreous fluid as a noninvasive alternative to the highly invasive oxygen electrodes used to measure retinal hypoxia,[1–3] bladder urine,[4] and urine in the renal pelvis to create a non-invasive detection of renal dysfunction,[5] and cerebrospinal fluid.[4,6] Additionally, measuring changes in R1 following the inspiration of increased fractions of oxygen is the basis for oxygen-enhanced MRI techniques,[7–9] which are used to study a range of conditions from tumor hypoxia[8,10,11] to lung disease.[12,13]

The linear relationship between the partial pressure of oxygen (PO_2) in a material and the resulting longitudinal relaxation rate (R1) has been measured in phantoms[2–4,6,14] and bodily fluids such as vitreous fluid.[2] The relationship between R1 and PO_2 has been modeled as for a paramagnetic contrast agent, $R1_{Ox} = R1_0 + r1_{Ox}*C$, where $R1_{Ox}$ is the relaxation rate in the solution with oxygen added, $R1_0$ is the relaxation rate in the solution without oxygen, C is the concentration of oxygen added, and $r1_{Ox}$ is the relaxivity of oxygen in that solution, which is dependent on the magnetic field and temperature.[15] Although this linear relationship has been demonstrated in phantoms and bodily fluids, studies on blood and tissues have sometimes reported so-called "contradictory" R1 changes, where either no change or a negative change in R1 is observed.[16,17] It has been hypothesized that the source of this contradictory R1 change is paramagnetic deoxyhemoglobin since there is a positive linear relationship between R1 and deoxyhemoglobin concentration, i.e., an inverse correlation with blood oxygen saturation.[18] The blood oxygen saturation, denoted by 'SO_2', is a measure of how much hemoglobin is currently bound to oxygen compared to how much hemoglobin remains unbound. In contrast, the partial pressure of oxygen (PO_2) in blood is a measure of the dissolved oxygen in the plasma.

To estimate changes in blood R1 following hyperoxia, Bluemke et al.[19] created a general model to estimate the R1 of blood, accounting for hematocrit, oxygen saturation (SO_2), the partial pressure of oxygen (PO_2), and magnetic field strength under both normal physiological and hyperoxic conditions. That model showed that there are two competing effects on blood R1 that arise from increasing oxygen levels (paramagnetic oxygen and paramagnetic deoxyhemoglobin) and that the effect on R1 due to deoxyhemoglobin dominates at SO_2 levels below 99%, thus inducing a negative ΔR1 in venous blood after breathing 100% oxygen. While this model does explain the negative ΔR1 measured by Vatnehol et al. in venous blood during oxygen delivery experiment,[16] it is not directly applicable to applications such as placental and tumor OE-MRI research where image voxels contain non-vascular tissue. In a tissue voxel, changing deoxyhemoglobin levels will only affect the portion of the voxel that is occupied by blood, and the R1 change of the tissue will dominate the remaining voxel volume. Therefore, in order to estimate the expected change in R1 of a tissue voxel, the blood model[19] must be extended to contain a tissue compartment.

In this paper, we present a three-compartment model for estimating the changes in R1 that could be expected in healthy, hypoxic, and necrotic tissues depending on field strength, blood oxygen saturation, blood volume, hematocrit, oxygen extraction fraction, and change in partial pressure of oxygen. Since modeling tissue oxygen diffusion and consumption is a broad, active research area with many different approaches, this model has been designed to make it possible for a researcher to easily substitute their preferred model for tissue oxygen diffusion and consumption and tailor this model to their tissue of interest. For this paper, the model incorporates the classic Krogh tissue cylinder model for oxygen diffusion and the commonly used Michaelis–Menten equation for oxygen consumption. Last, we demonstrate the use of this model for estimating the expected R1 changes in tissues from breathing increased levels of oxygen and compare the R1 estimations with literature empirical measurements from oxygen-enhanced MRI research.[8,10,11,20,21]

2 | THEORY

2.1 | Model background and overview

There have been two previous attempts at modeling the changes in tissue R1 following increased oxygen: both arise from the research field of OE-MRI.[22,23] In 2013, Holliday[22] used a two-compartment model of blood to estimate ΔR1 in a capillary given a change in capillary PO_2 (Equation 1) and used a Krogh tissue cylinder model to estimate the corresponding tissue ΔPO_2 (ΔPO_{2T}), allowing the ΔR1 in tissue to be calculated by Equation (2).

$$\Delta R1_{capillary} = \Delta PO_2 * r1_{Ox} + \Delta\,(1 - SO_2) * r1_{dHb} \quad (1)$$

$$\Delta R1_{tis} = \Delta PO_{2\,tis} * r1_{Ox}\,. \quad (2)$$

Holliday used the $r1_{dHb}$ at 1.5T reported by Blockley et al. ($0.11\,s^{-1}$).[18] The main limitation of Holliday's approach is that the resulting model contains many independently adjustable variables, such as the blood flow velocity, oxygen consumption rate, vessel geometry, and length of the

capillary. In practice, these variables are often impossible to measure in tissues.

In 2018, Kindvall[23] proposed a much simpler equation to estimate the expected R1 change in pulmonary OE-MRI, in which the total ΔR1 is separated into the expected ΔR1 of the arterial blood ($\Delta R1_{B,A}$), venous blood ($\Delta R1_{B,V}$), and tissue $\Delta R1_T$, and divided by 3 to yield an average ΔR1:

$$\Delta R1_{tis} = \frac{\Delta R1_{B,A} + \Delta R1_{B,V} + \Delta R1_T}{3}. \quad (3)$$

Kindvall then used empirical measurements from previous experiments to estimate ΔR1 at a set magnetic field strength (4.7T): the $\Delta R1_{B,A}$ and $\Delta R1_T$ were set to be the same values (0.2 s^{-1}), and $\Delta R1_{B,V}$ was estimated to be $-0.05\,s^{-1}$ based on the relaxivity of deoxyhemoglobin ($r1_{dHb}$) reported by Silvennoinen et al. ($0.35\,s^{-1}$) and a rough estimate of the expected change in venous deoxyhemoglobin levels.[24] The main insight provided by Kindvall's approach was the benefit of separating the R1 changes in arterial blood and venous blood to observe the negative ΔR1 induced in deoxygenated blood, as opposed to Holliday's approach of estimating the ΔR1 of the capillary blood. However, the division by 3 assumes a 66% blood volume fraction in the voxel, which is too high for most tissue voxels.

Last, some substantial limitations to both of these approaches are: (A) the equations used to calculate the blood ΔR1 were of unknown accuracy and were not compared with literature values, (B) they did not take into account the blood hematocrit levels, and (C) the equations were not adjustable for magnetic field strength, which has a considerable effect on the relaxivity of oxygen.[15]

Therefore, we propose a new three-compartment model that calculates the expected ΔR1 of the arterial blood ($\Delta R1_{B,A}$), venous blood ($\Delta R1_{B,V}$), and tissue $\Delta R1_T$ as separate compartments, and, following Holliday, uses a Krogh tissue cylinder model to estimate the corresponding tissue ΔPO_2 (ΔPO_{2T}). The model takes into account the magnetic field strength (B0), blood SO_2, blood volume fraction (BV), hematocrit (Hct), oxygen extraction fraction of the tissue (OEF), and changes in PO_2 in both the blood and tissue. Last, the model uses the blood volume fraction to calculate the resulting ΔR1 of the voxel ($\Delta R1_{voxel}$).

An overview of the model is illustrated in Figure 1. The model can be conceptually separated into four steps:

Step 1. Calculate PO_2 along the capillary. The $\Delta R1_{B,V}$ and $\Delta R1_T$ and $\Delta R1_{B,A}$ are all related by a calculation of the SO_2 or PO_2 along the capillary length, which is determined by the arterial PO_2 (PaO_2) and the OEF of the tissue.

Step 2. Calculate ΔPO_2 of each compartment. Knowing the PO_2 along the capillary allows the ΔPO_2 from oxygen administration to be calculated in the blood and tissue compartments, using the Krogh tissue cylinder to model the oxygen diffusion into the tissue, and the set OEF is related to the tissue oxygen consumption rate. The Krogh tissue cylinder radius is calculated from the set blood volume.

Step 3. Calculate ΔR1 of each compartment. Knowing the ΔPO_2 in each compartment allows: (A) the $\Delta R1_T$ to be calculated using the relaxivity of oxygen ($r1_{Ox}$) as a function of the magnetic field, using the equation for $r1_{Ox}$ by Bluemke et al.[15]; and (B) the ΔR1 of each blood compartment to be calculated using the Blood R1 model published by Bluemke et al.[19]

Step 4. Calculate ΔR1 of the voxel. Once the ΔR1 in each compartment is calculated, the set blood volume fraction (BV) is used to calculate the resulting ΔR1 of the voxel ($\Delta R1_{voxel}$).

The theory and reasoning behind each part of this model are provided in the following sections. The model has been provided as a public code repository, and a graphical overview of the inputs and outputs of each function created to implement this model is provided in Figure 1. This model was created as a set of Python functions, the overview of which is provided in Figure 2.

2.2 | Step 1: calculating PO_2 along capillary length

In this step, the PO_2 along the capillary is calculated using arterial oxygen content and oxygen extraction fraction inputs. The output of this step is the known SO_2 and PO_2 along the capillary, which can be calculated before and after the oxygen delivery or hyperoxic gas challenge.

The total concentration of oxygen (c) in the blood is the sum of the concentrations of bound and dissolved oxygen[25]:

$$c = c_{dissolved} + c_{bound} = \alpha_p * PO_2 + Hct * c_0 * SO_2, \quad (4)$$

where c is the total blood oxygen concentration, and c_0 is the concentration of oxygen per unit volume of red blood cells (RBCs) at maximal saturation, and a_p is the solubility of oxygen in plasma assuming 22.4 L/mol under normal conditions.[25] The total concentration (c) can also be referred to as the arterial oxygen content (C_aO_2) and venous oxygen content (C_vO_2). The following relationship between C_aO_2 and C_vO_2 defines the oxygen extraction

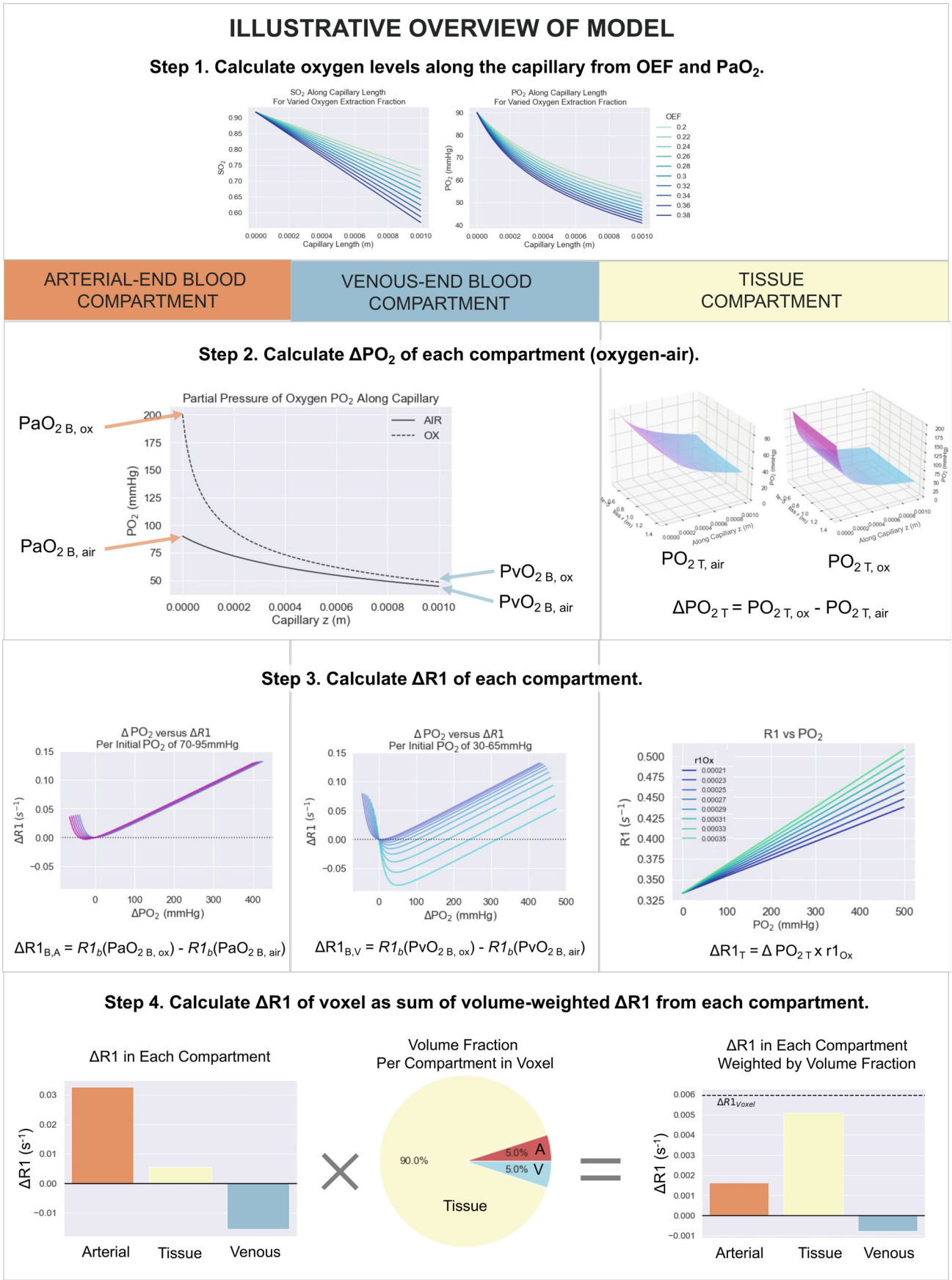

FIGURE 1 An illustrative overview of the three-compartment model, which can be separated conceptually into four steps as shown. The inputs and outputs of the functions used in each step are shown in Figure 2

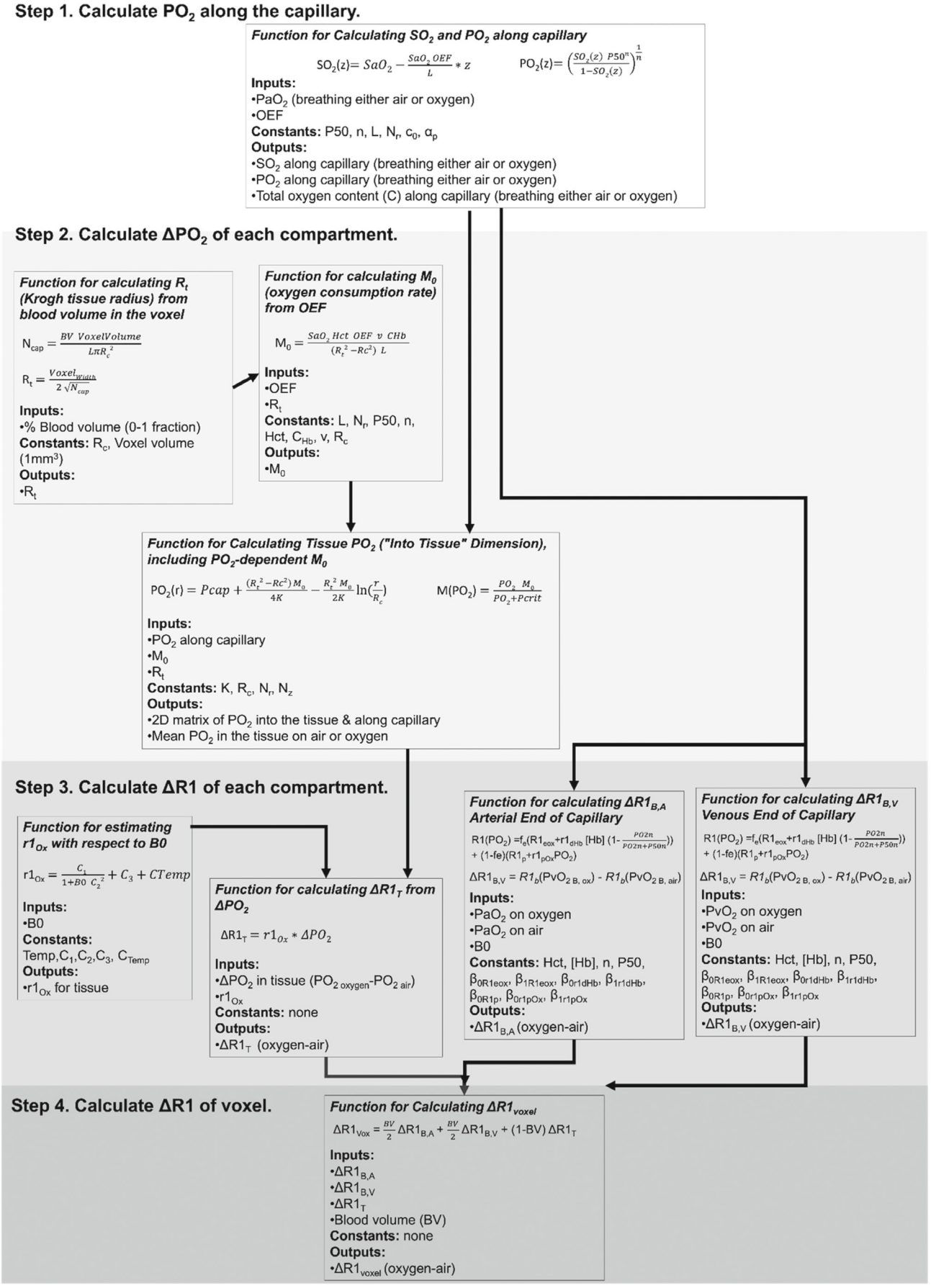

FIGURE 2 The inputs and outputs of each resulting function used in this model

fraction (OEF), which is the ratio of blood oxygen that tissue takes from the blood flow[26]:

$$OEF = \frac{C_aO_2 - C_vO_2}{C_aO_2}. \quad (5)$$

Using developed formalism from Gjedde et al.[27] and Rasmussen et al.,[28] assuming that the total oxygen extraction rises linearly with distance along the capillary, as established by Kety et al.,[29] the mean SO_2 in the capillary ($SO_{2\,cap,mean}$) can be defined in relation to OEF as[26]:

$$SO_{2_{cap,mean}} = SaO_2\left(1 - \frac{OEF}{2}\right). \quad (6)$$

The total oxygen content along the capillary can therefore be calculated for any given OEF (shown in Supporting Information Figure S1, which is available online) and initial SaO_2, PaO_2, or CaO_2 value, and find the resulting PO_2 and SO_2 along the capillary length by using Equation (6) and the Hill equation[30]:

$$SO_2(z) = SaO_2 - \frac{SaO_2\ OEF}{L} * z \quad (7)$$

$$PO_2(z) = \left(\frac{SO_2(z)\ P50^n}{1 - SO_2(z)}\right)^{(1/n)}, \quad (8)$$

where P50 is the oxygen tension when hemoglobin is 50% saturated with oxygen, and n is the Hill exponent for hemoglobin (typically 2.7).[30]

2.3 | Step 2: Estimating ΔPO_2 in the three compartments

2.3.1 | Blood compartments

In this model, the arterial PO_2 levels are chosen by the user. The arterial PO_2 following a hyperoxic gas challenge such as is used in OE-MRI, is estimated to increase from 90 mmHg to 600 mmHg based on empirical measurements,[31] and therefore this is used for the duration of this paper. The corresponding change in venous PO_2 will depend on the OEF, and is therefore calculated by the PO_2 values at the venous end of the capillary at baseline or with supplemental oxygen.

2.3.2 | Tissue compartment

Model for tissue oxygen diffusion

A wide variety of models for tissue oxygen diffusion and metabolism have been established, accounting for differing capillary networks, geometry, and other special features. For the purpose of this paper, we use the classic Krogh tissue cylinder model and common Michaelis–Menten equation for oxygen consumption rate, however any preferred tissue model can be substituted to calculate the resulting change in tissue oxygen levels (ΔPO_{2T}) from hyperoxia to use in Step 3. The Krogh-Erlang solution has the following assumptions, paraphrased from Goldman et al.[30]: (A) tissue oxygen consumption is constant and uniform; (B) tissue oxygen at the capillary wall equals average capillary PO_2; (C) tissue oxygen solubility and diffusivity are uniform (D) axial (or longitudinal) diffusion of oxygen is not significant; (E) all important microvascular oxygen transport phenomena are steady-state; (F) all capillaries are parallel, unbranched, and equally spaced; (G) all capillaries receive equal convective oxygen supply; (H) capillaries are the only microvessels that play a role in oxygen transport to tissue.

For steady state PO_2 in the tissue cylinder and a given capillary PO_2, the Krogh-Erlang solution is:

$$PO_2(r) = P_{cap} + \frac{M_0}{4K}\left(r^2 - R_c^2\right) - \frac{M_0R_t^2}{2K}\ ln\left(\frac{r}{R_c}\right) \quad (9)$$

where $PO_2(r)$ is the PO_2 at r in the tissue, R_c is capillary radius, R_t is the Krogh tissue radius, P_{cap} is the $PO_2(R_c)$ (partial pressure of oxygen at the capillary radius), r is the radial coordinate, M_0 is the maximum tissue oxygen consumption rate, and K is the Krogh diffusion constant $K=Da_T$, where D is the tissue oxygen diffusivity and a_T is the tissue oxygen solubility.[30] The behavior of Equation (9) for different levels of P_{cap} is shown in Supporting Information Figure S2A.

Model for tissue oxygen consumption

As discussed by Goldman et al.,[30] one important modification commonly made to the Krogh cylinder model is the addition of PO_2-dependent tissue oxygen consumption. The most common model, Michaelis–Menten, calculates the oxygen consumption rate by the following equation:

$$M\left(PO_2\right) = \frac{M_0\ PO_2}{PO_2 + P_{crit}} \quad (10)$$

where tissue oxygen consumption rate $M(PO_2)$ is found to be approximately constant for tissue PO_2 above a certain value (P_{crit}), and below this value, the oxygen consumption drops off sharply to zero.[30] The behavior of Equation (10), and the effect of varying P_{crit}, is shown in Supporting Information Figure S2B. Therefore, in this manuscript, the M_0 constant in Equation (7) has been replaced with the function $M(PO_2)$ (Equation 10).

Estimating R_t from blood volume

Equation (9) requires knowledge of the Krogh tissue radius (R_t), which can be estimated per the chosen blood volume (BV). Based on the Krogh assumptions above, we can model the capillaries as cylinders that are parallel, unbranched, and equally spaced throughout the 3D voxel (illustrated in Supporting Information Figure S3). Capillary length can range from 0.5–1.5 mm, so for simplicity in modeling a 1 mm^3 voxel, we will assume a capillary length of 1 mm. The volume of one cylindrical capillary is:

$$V_{cap} = \pi R_c^2 L. \tag{11}$$

The estimated blood volume can be related to the capillary density in the voxel through the following equation from which N_{cap} can be calculated (assuming a constant R_c and L):

$$BV = \frac{N_{cap} x V_{cap}}{V_{voxel}}. \tag{12}$$

In a cross-section, based on the sixth assumption from the Krogh-Erlang solution, the number of capillaries (N_{cap}) are spaced evenly across the width and length of the voxel cross-section. Therefore, R_t can be found by using the following equation:

$$Voxel_{width} = 2R_t * \sqrt{N_{cap}}. \tag{13}$$

Estimating Oxygen Consumption Rate M_0 from OEF and R_t

Using the Krogh-Erlang solution (Equation 9) also requires knowledge of the maximum tissue oxygen consumption rate, M_0. Once R_t is found, we can derive M_0 from the OEF using the following logic and assumptions. It is important to note that in order for the assumptions of the following equations to be valid, M_0 must be calculated in the normoxic state (i.e., the patient is breathing air). Under this assumption, the SO_2 along the capillary can be calculated using the linear equation[30]:

$$SO_2(z) = SaO_2 - \frac{\left(R_t^2 - R_c^2\right)\ M_0}{Hct\ C_{Hb}\ v} * z. \tag{14}$$

Using Equation (6), which relates mean SO_2 to the OEF, we can create a linear equation of SO_2 along z, the mean SO_2 in the capillary ($SO_{2\ cap,mean}$) will be equal to the linear Equation (14) at 0.5 L. Therefore, M_0 can be related to OEF using the following steps:

$$\begin{aligned} SO_{2_{cap,mean}} &= SaO_2 * \left(1 - \frac{OEF}{2}\right) = SO_2(0.5L) \\ &= SaO_2 - \frac{\left(R_t^2 - R_c^2\right)\ M_0}{Hct\ \ C_{Hb}\ v} * 0.5L \end{aligned} \tag{15}$$

which can be rearranged to calculate M_0:

$$M_0 = \frac{OEF\ Hct\ C_{Hb}\ v\ SaO_2}{\left(R_t^2 - R_c^2\right)\ L}. \tag{16}$$

Finally, with M_0 and R_t estimated from the OEF and blood volume, the tissue PO_2 (into-tissue axis) can be calculated. Since the PO_2 along the capillary (P_{cap}) on air and oxygen breathing is known from Step 1, the PO_2 throughout the Krogh cylinder can be calculated for both normoxic and hyperoxic situations (shown in Supporting Information Figure S4).

2.4 | Step 3. Calculating ΔR1 in the three compartments

2.4.1 | Blood compartments

The ΔR1 induced from supplemental oxygen in the arterial ($\Delta R1_{B,A}$) and venous ($\Delta R1_{B,V}$) blood compartments can both be calculated from the following equation

$$\Delta R1_B = R1_b\left(PO_{2,ox}\right) - R1_b\left(PO_{2,air}\right) \tag{17}$$

where $R1_b(PO_2)$ is the general equation for calculating the R1 of blood by Bluemke et al.[19] (shown in Figure 3):

$$\begin{aligned} R1_b\left(PO_2\right) = f_e &\left(R1_{eox} + r1_{dHb}[Hb]\left(1 - \frac{PO_2^n}{PO_2^n + P50^n}\right)\right) \\ &+ (1 - f_e)\left(R1_p + r1_{pOx} PO_2\right) \end{aligned} \tag{18}$$

where $R1_b$ is the relaxation rate of whole blood, $R1_{eox}$ is the relaxation rate of erythrocytes when SO_2 = 100%, [Hb] is the mean corpuscular hemoglobin concentration (5.15 mmol Hb tetramer/L plasma), $r1_{dHb}$ is the molar relaxivity of deoxyhemoglobin (in s^{-1} L plasma in erythrocyte/mmol Hb tetramer), n is the Hill exponent for hemoglobin (typically 2.7),[30] $R1_p$ is the longitudinal relaxation rate of plasma (s^{-1}), and $r1_{pOx}$ is the relaxivity of dissolved oxygen in the plasma in s^{-1} $mmHg^{-1}$ oxygen. The variable f_e is the fraction of water in whole blood that resides in erythrocytes (0–1), which is described by the equation:

$$f_e(Hct) = \frac{W_{RBC} Hct}{W_{RBC} Hct + W_{plasma}(1 - Hct)} \tag{19}$$

where Hct is the hematocrit (0–1), W_{RBC} is the volume fraction of water within the erythrocyte (typically valued at 0.70 due to hemoglobin occupying approximately 30% of the erythrocyte volume), and W_{plasma} is the volume fraction of water within the plasma (typically valued at 0.95,

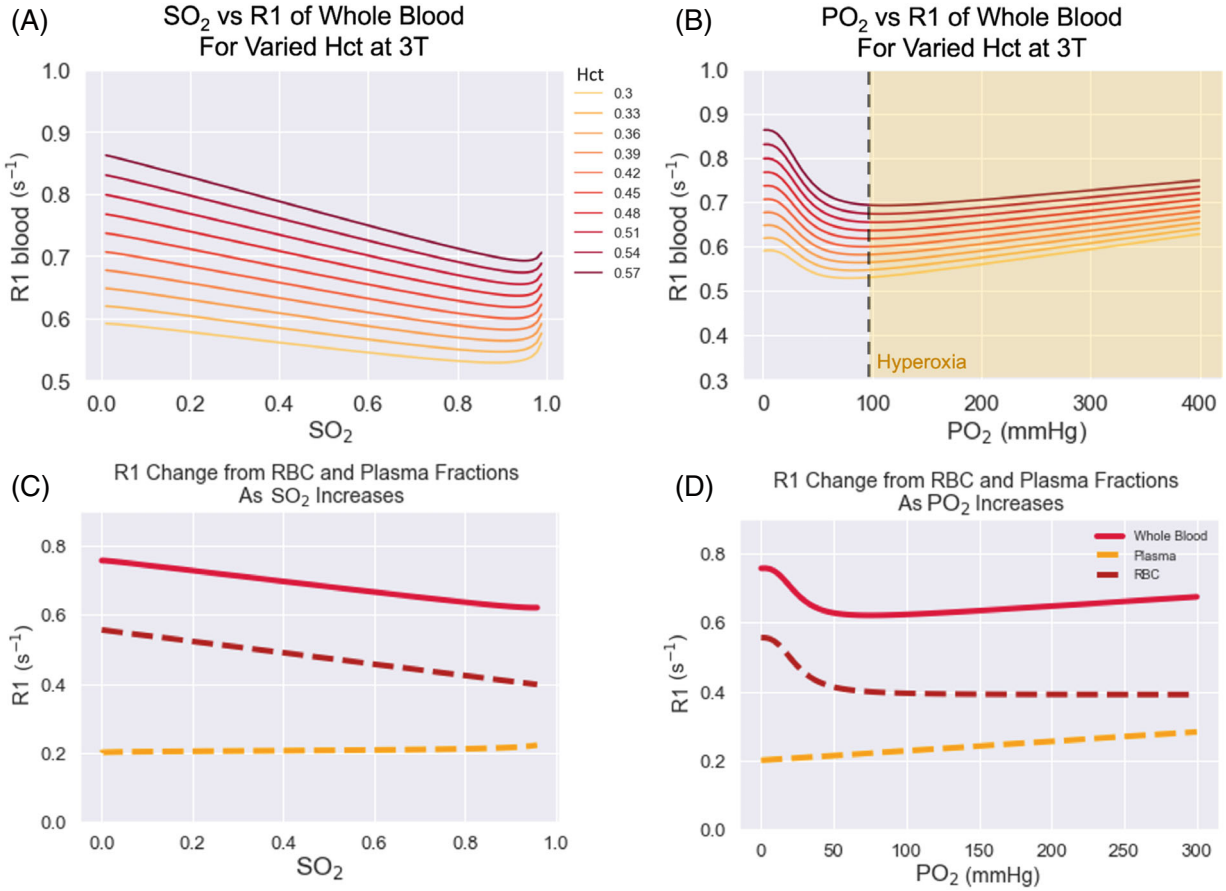

FIGURE 3 Plots with simulated data to illustrate the behavior of the model published by Bluemke et al., showing PO_2 vs R1 (A) and SO_2 vs R1 (B) for a range of hematocrit values (0.3–0.57) at 3T. To show the behavior of the two compartments of the model, the plasma fraction (yellow) and erythrocyte fraction (maroon) are shown separately as SO_2 increases (C) and PO_2 increases (D), with B0 = 3T, Hct = 0.42

where the other 5% volume is occupied by plasma proteins such as albumin).[32] In addition, Bluemke et al.[19] modeled $R1_{eox}$, $R1_p$, $r1_{dHb}$, and $r1_{pOx}$ to have a linear dependence on B0 (where β_0 and β_1 are the y-intercept and slope for the linear fit):

$$R1_{eox}(B0) = \beta_{0,R1_{eox}} + \beta_{1,R1_{eox}} B0 \quad (20)$$

$$R1_p(B0) = \beta_{0,R1_p} + \beta_{1,R1_p} B0 \quad (21)$$

$$r1_{dHb}(B0) = \beta_{0,r1_{dHb}} + \beta_{1,r1_{dHb}} B0 \quad (22)$$

$$r1_{pOx}(B0) = \beta_{0,r1_{pOx}} + \beta_{1,r1_{pOxB0}} B0\,. \quad (23)$$

The values used for all empirically derived parameters and constants in the blood model are listed in the original publication.[19] The behavior of this model is shown in Figure 3.

2.4.2 | Tissue compartment

Between the air and oxygen states, the only paramagnetic factor changing in the tissue compartment is the concentration of oxygen dissolved either intracellularly or interstitially. Therefore, the ΔPO_{2T} calculated in Step 2 can be used to calculate the $\Delta R1_T$ using the following equation

$$\Delta R1_T = r1_{Ox} * \Delta PO_{2\,T} \quad (24)$$

where the relaxivity of oxygen, $r1_{Ox}$, is dependent on field strength and calculated using the empirical model for $r1_{Ox}$ published by Bluemke et al.[15] (shown in Figure 4):

$$r1_{Ox} = \frac{C_1}{1 + C_2 B0^2} + C_3 + C_{Temp} * T \quad (25)$$

where the empirically derived constants are set to the parameters reported by Bluemke et al.,[15] and in the context of this tissue model, temperature is assumed to be 37°C.

2.5 | Step 4. Calculating weighted voxel ΔR1

Last, the model uses the blood volume fraction (BV) to calculate the resulting ΔR1 of the voxel ($\Delta R1_{voxel}$), assuming

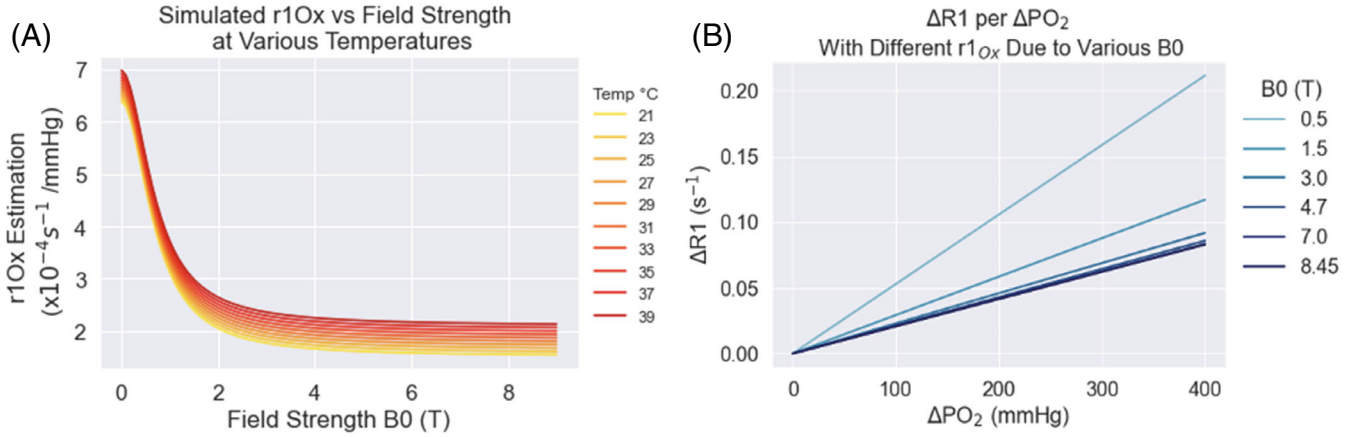

FIGURE 4 Simulated data to illustrate the effect of field strength on the relaxivity of oxygen ($r1_{Ox}$) according to the model by Bluemke et al. (for a variety of temperatures) (A), and the resulting effect on R1 from different strengths of $r1_{Ox}$ within a range of commonly used main magnetic fields (B0) (B)

equal fractions of arterial and venous blood are present in the voxel, using the following equation:

$$\Delta R1_{voxel} = \left(\frac{BV}{2}\right)\Delta R1_{B,A} + (1 - BV)\Delta R1_T + \left(\frac{BV}{2}\right)\Delta R1_{B,V}\ . \tag{26}$$

By keeping the arterial and venous changes separate, the +ΔR1 in more oxygenated blood will be accounted for in the "arterial end" compartment and the −ΔR1 in the less oxygenated blood will be accounted for in the "venous end" section. Ultimately, the large volume fraction of tissue contributes the most to the final $\Delta R1_{voxel}$ (see schematic in Supporting Information Figure S5).

3 | METHODS

3.1 | Applying model to simulate ΔR1 from OE-MRI

3.1.1 | Model variables and constants

To demonstrate the application of this model, the five independent variables that vary between different types of tumor tissues, patients and experiments were: the magnetic field B0, hematocrit, oxygen extraction fraction, blood volume in the voxel, and P_{crit} — the ranges of these values used to produce the R1 estimates are listed in Table 1. Next, there are four dependent variables that are calculated from the independent variables: the fraction of erythrocytes in whole blood f_e is calculated from hematocrit; the $r1_{Ox}$ is calculated from B0; the Krogh tissue radius R_t is calculated from OEF and blood volume, and the tissue oxygen consumption rate is calculated from OEF, R_t, and P_{crit} (shown in Table 2). Last, the constants used for the remaining parameters were sourced from the literature and listed in Table 3.[25,30,33,34]

The chosen "tissue types" to simulate were: healthy brain tissue, and tumor regions of "vascular periphery," "necrotic tissue," "tissue with high metabolism" to simulate hypoxic regions (split into "more hypoxic" and "less hypoxic" by higher and lower blood volume ranges), and "tissue with normal metabolism" to simulate the regions of the tumor which are not hypoxic. To select ranges for OEF, P_{crit}, and blood volume that have already been approved in peer-review were used, such as the values published in a computational model for tumor oxygenation by Welter et al. were used,[25] or published values that were measured experimentally. For OEF: Welter et al. report an OEF in healthy breast tissue of 0.11 ± 0.09, and breast tumor tissue of 0.34 ± 0.1; Cho et al.[35] report an OEF in healthy brain tissue of $34.2 \pm 2.6\%$; and necrotic tissue was assumed to be very low, between 0.02 and 0.05. For blood volume: Leenders et al. measured the blood volume in healthy brain tissue to be $5.2\% \pm 1.4\%$ and $2.7 \pm 0.6\%$ for gray and white matter, respectively[36]; Welter et al. report that using MRI and a brain tumor animal model, BV of tumor tissue was $5.3\% \pm 0.6\%$ which is used as the "low blood volume range," and Qi et al.[37] measured $13\% \pm 4.1\%$ blood volume in VX2 squamous cell tumors, which is used as the "high blood volume" range; for necrotic tissue, a 0.01% blood volume is used, i.e., almost no blood compartment is present. Last, Welter et al. report that literature values of P_{crit} range from 1-4 mmHg, and Welter et al. lowered P_{crit} for tumor tissue by ½ due to resistance to hypoxia; this corresponds with reports from Honig and Gayeski, who report tumor P_{crit} as 0.5 mmHg.

For the dependent variables, the resulting range of R_t calculated from the range of BV values chosen in Table 1 is $1.07–4.43 \times 10^{-5}$ m, which is similar to ranges reported

TABLE 1 Five independent variables that vary between different types of tumor tissues, patients, and experiments

Variable Meaning	Variable Name	Healthy Brain Tissue	Tumor Vascular Periphery *No Tissue Compartment*	Tumor Tissue with High Metabolism i.e., Hypoxic *2 types: Low BV and High BV*	Tumor Tissue with Normal Metabolism	Tumor Necrotic Tissue *No Blood Compartments*	Units
Main magnetic field of MRI	B0	1.5, 3, 4.7, 7					T
Hematocrit	Hct	Total range: 0.36–0.50 Female range: 0.36–0.48 Male range: 0.41–0.50					0–1 Volume fraction
Oxygen extraction fraction	OEF	0.31–0.37	0.24–0.44		0.02–0.2	0.02–0.05	0–1 Fraction
Blood volume in voxel	BV	0.02–0.07	1.0 (100% blood volume, no tissue compartment)	Low BV range = 0.047–0.059 High BV range = 0.09–0.17	0.047–0.059	0.001 (0.1% blood volume, i.e., no blood compartment)	0–1 Volume fraction
The PO_2 value above which the tissue oxygen consumption rate is relatively constant	P_{crit}	1–4	N/A	0.5–2			mmHg

Note: The chosen ranges of these values used to produce the simulated results in this paper are listed.

TABLE 2 Four dependent variables that are calculated from the independent variables listed in Table 1

Parameter meaning	Parameter name	Value or range used	Units
Fraction of erythrocytes in whole blood	f_e	Calculated by Equation (19) as a function of Hct, W_{RBC} and W_{plasma}	0–1 Volume fraction
Relaxivity of oxygen	$r1_{Ox}$	Calculated by Equation (25) as a function of B0 and temperature (set to 37 °C for tissue model)	s^{-1} $mmHg^{-1}$
Krogh tissue radius	R_t	Determined by the blood volume	m
Tissue oxygen consumption	M_0	Determined by the OEF and the R_t	mlO_2 ml^{-1} s^{-1}

TABLE 3 Constants used for the remaining parameters of the model

Constant meaning	Name	Value used (units)	Source
Oxygen tension when hemoglobin is 50% saturated with oxygen	P50	37 (mmHg)	Goldman 2008
Hill coefficient	n	2.7 (unitless)	Goldman 2008
Plasma O_2 solubility	a_p	3.1×10^{-5} (mlO_2 ml^{-1} $mmHg^{-1}$) **assuming 22.4 L/mol under normal conditions*	Welter 2016
Hemoglobin binding capacity (Hüffner factor)	C_{Hb}	1.36 (mlO_2 g^{-1})	Welter 2016
Concentration of oxygen per unit volume of RBCs at maximal saturation: calculated as the product of the hemoglobin binding capacity C_{Hb} and the mean corpuscular hemoglobin concentration [Hb]	c_0	Calculated from $c_0 = C_{Hb} \times [Hb]$ $= 1.36\ mlO_2/g \times 0.43\ g/mL$ $= 0.5\ (mlO_2\ ml^{-1})$	Welter 2016
Tissue O_2 solubility	a_T	2.8×10^{-5} (mlO_2 ml^{-1} $mmHg^{-1}$)	Welter 2016
Tissue O_2 diffusivity	D_T	2.41×10^{-9} ($m^2 s^{-1}$)	Welter 2016
Capillary length	L	0.001 (m)	Less 1991
Capillary radius	R_c	3.5×10^{-6} (m)	Less 1991
Capillary velocity	v	0.00079 ($m\ s^{-1}$)	Ivanov 1981

such as 4×10^{-5} m[38] and 2.5×10^{-5} m.[39] Likewise, the resulting range of M_0 calculated from the range of OEF chosen in Table 2 is 1.2×10^{-5}–3.5×10^{-4}, which is consistent with the reported M_0 values of 6×10^{-5} and 2.4×10^{-4} $mlO_2/mL/s$ for normal tissue and tumor tissue, respectively, used by Welter et al.[25]

3.1.2 | Comparison with empirical OE-MRI results

Empirical OE-MRI measurements by Winter et al.,[10] Bhogal et al.,[20] O'Connor et al.,[11] Little et al.,[8] and Muir et al.[21] were used for comparison because they either estimated or measured the PaO_2 change induced by their hyperoxic gas challenge. Altogether, these studies provided measurements in "healthy brain tissue,"[20] "vascular periphery," "tumor core," "necrotic tissue,"[10] and whole tumor region of interest (ROI) measurements from clinical patient data by O'Connor et al.,[11] and Little et al.[8] As it is not possible to know the composition of the whole tumor ROIs reported, the simulated ΔR1 for each possible tumor tissue type is calculated for comparison, and it is assumed that the empirical whole tumor ROI should fall within that range of ΔR1.

In the measurements from Winter et al., the exact definition of the "necrotic" versus "central tumor" regions is defined as follows[10]: the necrotic core was characterized as exhibiting hypo-intensity on post-contrast gadolinium-enhanced T1-weighted imaging, suggesting it was avascular, and the necrotic nature of this region was confirmed by histology. In contrast, the "central tumor" was defined as tumor tissue excluding the enhancing vascular rim and excluding necrotic tissue, if any.

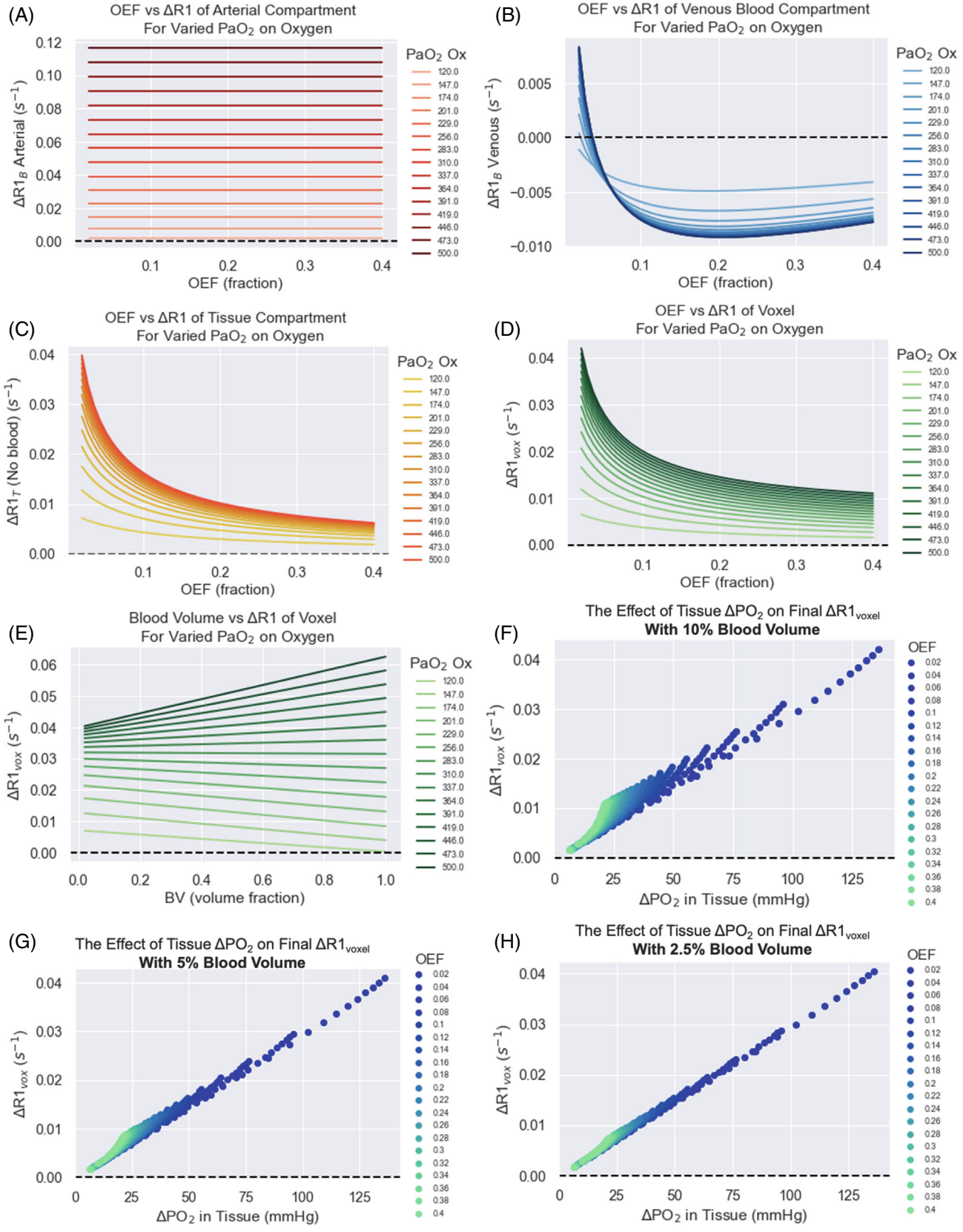

FIGURE 5 Simulated data showing the effect of OEF on the ΔR1 of the arterial blood (A), venous blood (B), and tissue compartments individually (C), and total voxel ΔR1 (D) for varied PaO_2 changes induced from increased oxygen breathing, with blood volume set to 10%. E, The corresponding effect of varying blood volume with a set OEF (OEF = 0.2) is shown. F–H, Simulated data showing the relationship between ΔPO_2 in the tissue compartment and $\Delta R1_{voxel}$, for 10% (F), 5% (G), and 2.5% (H) blood volume. The data points are colored by the OEF (0.02–0.40) used in that $\Delta R1_{voxel}$ calculation (see OEF legend). All simulations in this figure used B0 = 1.5T

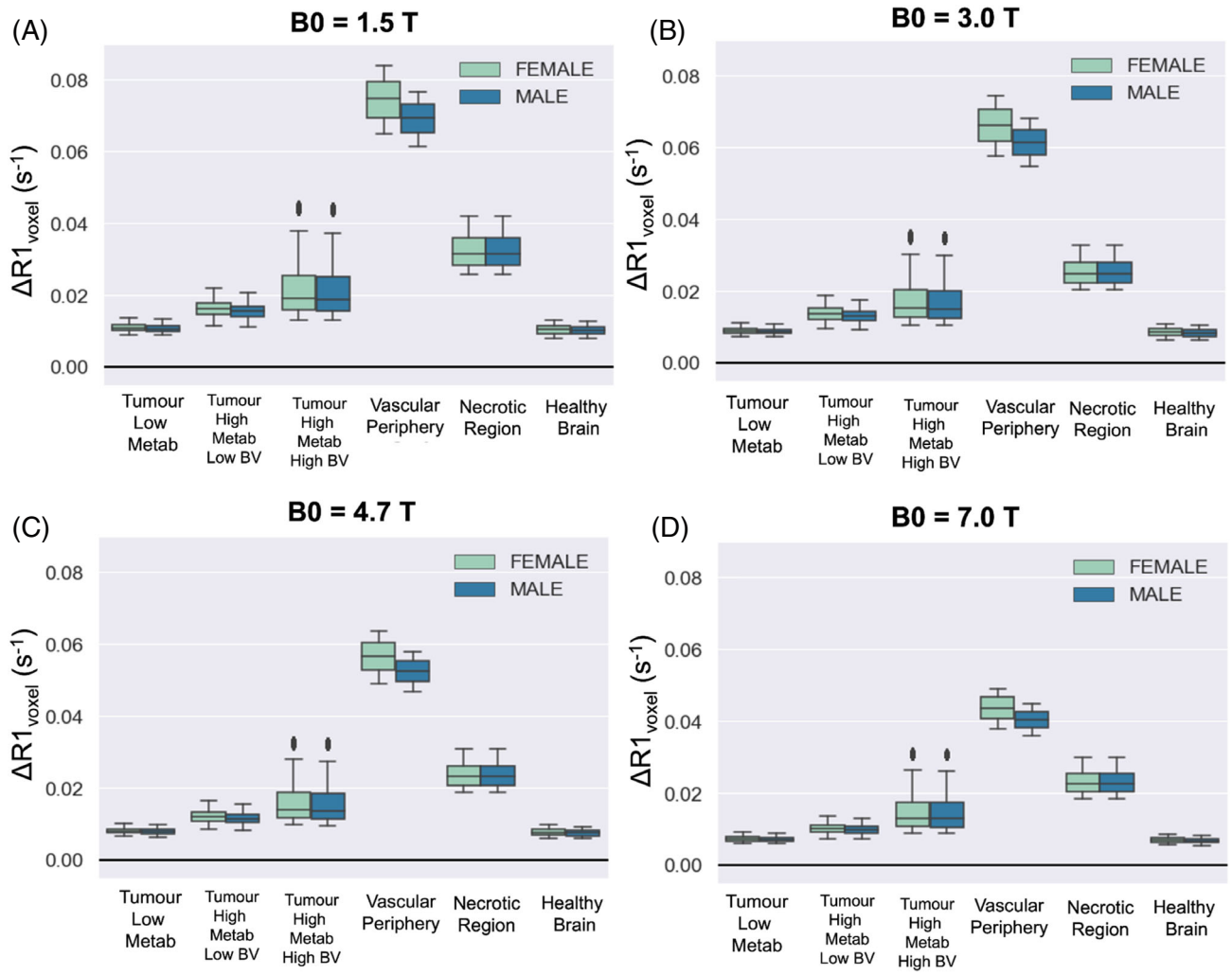

FIGURE 6 The resulting ΔR1 from a hyperoxic gas challenge calculated from this model, calculated using all combinations of the chosen range of Hct (using the female and male ranges for hematocrit separately), OEF, BV, P_{crit} listed in Table 1 for each respective tumor tissue type, with B0 set to 1.5T (A), 3T (B), 4.7T (C), 7T (D)

4 | RESULTS

To visualize the relationship between the independent variables, dependent variables, and ΔR1, the following plots were produced. The effect of all combinations of blood volume and OEF on the baseline tissue PO_2 (mean and minimum) and maximum oxygen consumption rate is shown in Supporting Information Figure S6. The effect of OEF on the ΔR1 of the venous, arterial, and tissue compartments individually, for varied PaO_2 changes induced from oxygen, is shown in Figure 5A–C, and the resulting ΔR1 for the voxel is shown in Figure 5D,E (all simulated at 1.5T). In this model, there is an inverse mathematical relationship between blood volume and the Krogh Radius R_t (shown in Supporting Information Figure S3), and therefore blood volume has an effect on the M_0 (see Supporting Information Figure S6C), where M_0 increases with blood volume fraction. In our model, blood volume is considered to be the independent variable while M_0 is dependent, however in biological reality, this is a highly intertwined feedback relationship where tissues with high metabolism recruit more blood vessels.[40] Blood volume also has an effect on the final $\Delta R1_{voxel}$ (see Figure 5D,E), which is due to the increased contributions from the arterial and venous components in Step 4 of the model. Interestingly, when there has been a smaller change in PaO_2 (i.e., less oxygen administered), the increase in the blood volume fraction allows the negative ΔR1 from the venous component to decrease the ΔR1 of the voxel, whereas this becomes dominated by the high increase in ΔR1 from the arterial component as more oxygen is administered.

In this model, the OEF chosen has a large effect on $\Delta R1_{voxel}$, which can be seen clearly in Figure 5D,E. Figure 5A,E shows that as OEF increases – in other words,

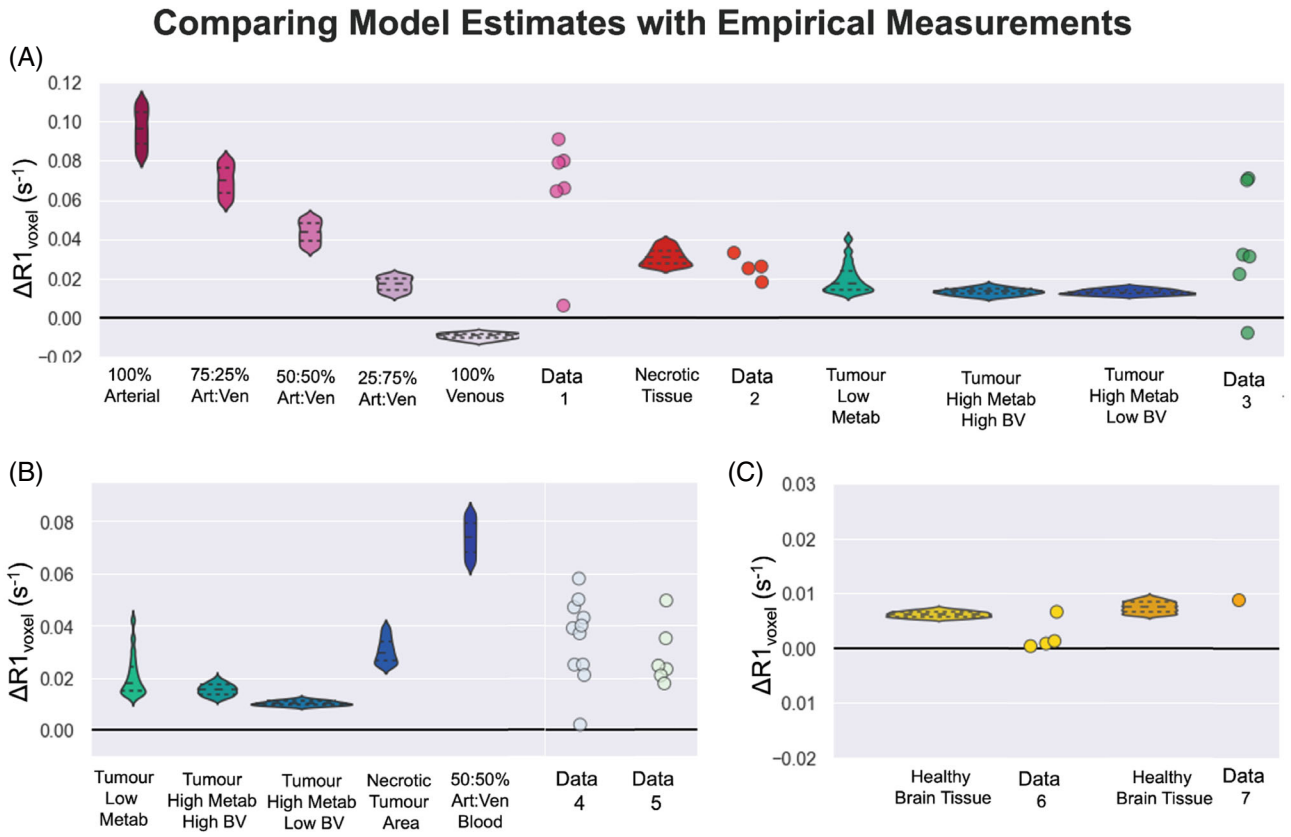

Source of Empirical Measurements		
Label	Reference	Details
Data 1	Winter et al. 2011	"Vascular Periphery" of rabbit VX2 carcinoma tumours, 1.5T; $PaO_{2,air}$= 83 mmHg; $PaO_{2,ox}$= 428 mmHg
Data 2		"Necrotic" region of rabbit VX2 carcinoma tumours, 1.5T; $PaO_{2,air}$= 83 mmHg; $PaO_{2,ox}$= 428 mmHg
Data 3		"Tumour core" region of rabbit VX2 carcinoma tumours, 1.5T; $PaO_{2,air}$= 83 mmHg; $PaO_{2,ox}$= 428 mmHg
Data 4	O'Connor et al. 2009	Whole tumour ROI of patients with advanced cancer of the abdomen and pelvis, 1.5T; $PaO_{2,air}$= 98 mmHg; $PaO_{2,ox}$= 600 mmHg
Data 5	Little et al. 2018	Whole tumour ROI of patients with renal cell carcinoma, 1.5T; $PaO_{2,air}$= 98 mmHg; $PaO_{2,ox}$= 600 mmHg
Data 6	Bhogal et al. 2017	Healthy human brain ROI, 7T, $PaO_{2,air}$= 109 mmHg; $PaO_{2,ox}$= 500 mmHg
Data 7	Muir et al. 2016	Healthy human brain ROI, 7T, $PaO_{2,air}$= 98 mmHg; $PaO_{2,ox}$= 750 mmHg

FIGURE 7 Plots containing seven sets of empirical ΔR1 measurements, alongside the respective simulated ΔR1 according to the B0, PaO_2, and tissue type

as a higher fraction of oxygen is extracted from the tissue between the arterial and venous ends – there will be a lower change in PO_2 in the tissue (and hence smaller $\Delta R1_T$), which is the largest contributor to the overall ΔR1 of the voxel. Last, the relationship between ΔPO_2 in the tissue compartment and $\Delta R1_{voxel}$ is shown in Figure 5F-H.

The resulting ΔR1 calculated from this model is plotted in Figure 6, calculated using different field strengths, and using all combinations of the chosen range of Hct, OEF, BV, P_{crit} listed in Table 1 for each respective tumor tissue type. Since hematocrit levels can vary between sexes, the results from using the female and male ranges for hematocrit have been shown separately to examine the expected difference in ΔR1. In this simulation, the largest difference in ΔR1 between the sexes was 0.0045 s^{-1}, which occurred in the vascular periphery due to containing the highest percentage of blood component and therefore most affected by differences in hematocrit. The difference in ΔR1 between the sexes was negligible in the other simulated tissue types.

For a rough quantitative comparison, empirical $_{\Delta R1}$ measurements from six tissue types, alongside the respective simulated ΔR1 according to the B0, PaO_2 and tissue type, are shown in Figure 7. It is not possible to know the composition of the whole tumors ROIs reported by O'Connor et al.[11] and Little et al.,[8] or the "tumor core" reported by Winter et al.,[10] however, each data point for empirical tumor ΔR1 falls within the range of ΔR1 simulated for each possible tumor tissue type; therefore, these whole tumor ROIs could reasonably be the sum of a

composition of these different tumor tissue types. One notable exception to this is one "tumor core" data point reported by Winter et al.,[10] which reaches a negative ΔR1 close to that of pure venous blood.

5 | DISCUSSION

In this paper, we propose a three-compartment model for estimating the changes in R1 that could be expected in tumor tissues depending on field strength, blood SO_2, blood volume, hematocrit, oxygen extraction fraction, and changes in PO_2 in both the blood and tissue. This model has been developed with the aim of estimating the expected ΔR1 induced by the oxygen delivery in a voxel containing tumor tissue, however, it is generally applicable to OE-MRI research as well and has been designed to make it possible for a researcher to easily substitute their preferred model for tissue oxygen diffusion and consumption and make this model tailored to their tissue of interest, for example, placenta or liver.

Interestingly, the relationship between ΔPO_2 in the tissue compartment and $\Delta R1_{voxel}$ (Figure 5F-H) shows that the linear relationship between ΔPO_2 and $\Delta R1_{voxel}$ seen in phantoms almost holds true in tissue voxels containing lower blood volume; however, in voxels containing higher blood volume, the ΔR1 contribution from the blood compartment interrupts the linear relationship. This suggests that despite the influence of deoxyhemoglobin changes, measuring ΔR1 does provide an indication of the final change in PO_2 in the tissue. In practice, the efficiency of the oxygen delivery to the tissue via inhalation of increased oxygen fraction can be affected by by many factors, and therefore for convenience, Figure 5D simulated a large range of PaO_2 changes (120-500 mmHg) where the resulting change in the R1 (at 1.5T) of the voxel can be seen for each respective PaO_2. In addition, Figures 5F-H display the estimated corresponding ΔR1 for a large range of levels of changes in tissue PO_2 at 1.5T, allowing for a convenient estimate of the corresponding ΔR1 by quickly viewing the data points in Figure 5F-H.

It is known that the values estimated by the $r1_{Ox}$ model and R1 Blood models by Bluemke et al.[15,19] both agree well with empirical measurements (R^2 = 0.93 and 0.93); however, since the tissue compartment of this model contains variables that were not measured at the time of OE-MRI data collection (i.e., hematocrit, changes in arterial PO_2, tumor blood volume), it is not possible to quantitatively compare the model ΔR1 predictions to the measured ΔR1 with metrics such as R^2 and MSE. Instead, we used a variety of reported ΔR1 from OE-MRI literature to gain a rough estimation of the accuracy of this model: qualitative ΔR1 responses, categorized by different tumor tissue types by the authors of the OE-MRI literature, are listed in Supporting Information Table S1. Overall, the simulated ΔR1 for each tissue type shown in Figure 6 does correspond with observations from OE-MRI literature: as seen in experiments by Winter et al.,[10] the "vascular periphery" shows greater +ΔR1 than the "tumor core" and "necrotic" regions, and the "necrotic" regions show a greater +ΔR1 than the "tumor core" but less than "vascular periphery." This is consistent with the distinctions between these three regions defined by Winter et al. — (1) necrotic region is avascular and filled with fluid, (2) the central tumor is cell-dense and has much lower vascularity than vascular periphery. As observed in experiments by Burrell et al.,[41] the "less hypoxic" tumor type shows greater +ΔR1 than the "more hypoxic" tumor type. Last, in these simulations, the healthy brain tissue is predicted to show a very small ΔR1 that might end up 'not detectable', as observed by Bhogal et al.[20]

For a select few OE-MRI studies that did report either measured or estimated PaO_2 changes, the simulated ΔR1 from the model did result in ΔR1 values that were in good agreement with the empirical data (Figure 7). The values for brain tissue and necrotic tissue were particularly accurate, and although it Is not possible to know the composition of the whole tumors ROIs, "vascular periphery," or "tumor core," each data point for empirical tumor ΔR1 fell within the range of ΔR1 simulated for each possible tumor tissue type. Therefore, the empirical ΔR1 could reasonably be the sum of a composition of these different tumor tissue types.

This model may be useful for OE-MRI researchers looking to predict the effect of certain factors, such as hematocrit. It is interesting that hematocrit differences in the male and female populations did have a slight effect on ΔR1 when the voxel contained larger blood volumes. In fact, this predicted difference has been empirically observed in lung tissue — where blood volume is approximately 33%–36%[42] — Kindvall et al.[12] reported that age and sex were all predictors of ΔR1 in lung tissue, likely due to the hematocrit differences.

5.1 | Limitations

It is currently difficult to quantify the agreement of this model with the empirical data, and the model still includes some constants and variables that cannot be measured in individual patients, although it has been designed so that the independent variables are either known (such as B0) or can be measured via a non-imaging method (i.e., arterial PO_2, hematocrit), or through another imaging method (i.e., measuring blood volume or OEF). Testing whether it would be possible to use OEF or blood volume

measurements from another imaging modality is beyond the scope of this paper, however, in the future, as methods for measuring blood volume or OEF continue to advance, this connection could prove useful in future work. In the future, it is possible that combining R1 measurements with other MRI techniques such as R2* or oxygen-17 gas[43] could improve the accuracy and robustness for monitoring oxygenation.

In addition, there may be unpublished raw datasets from former OE-MRI studies held by other research groups where arterial PO_2 was measured but perhaps not reported. We welcome other researchers to test the predictions of this model against a larger sample size of data — this would greatly improve confidence in this model before it is applied in oxygen-enhanced MRI studies.

Another limitation is that, in this current model, the arterial blood volume has been set to be equal to the venous blood volume — this will not be true for all voxels. Since we have provided the open-source code for the model, future researchers are welcome to adjust this parameter if they have more information about the ratio of arterial and venous blood in their voxels of interest.

The the parameters for the $r1_{Ox}$ model by Bluemke et al.[15] were created by compiling empirical measurements of the relaxivity of oxygen over 50 y of MRI research in phantoms, saline and water solutions, vitreous fluid, and plasma, and fitting these data to a Lorentzian equation that fit $R^2 = 0.93$. Of course, the $r1_{Ox}$ in these solutions may be slightly different than the $r1_{Ox}$ in tissues. Indeed, the $r1_{Ox}$ may vary between tissues as well. However, we believe the $r1_{Ox}$ derived from this empirically driven model will better represent the $r1_{Ox}$ in tissue than using any single $r1_{Ox}$ datapoint measured in saline or water, as has been common practice in previously published work using $r1_{Ox}$ values for various calculations.[3,5,14,22,23,44,45]

This model contains fewer independent variables than the model by Holliday et al.,[22] but considerably more variables than the simple equation proposed by Kindvall et al.[23] Ideally, the outputs of these three models could be compared; however, since they are so different and contain such different parameters, it is difficult to choose the variable "settings" at which to compare them. For example, this new model adjusts all field-dependent parameters according to field strength, while both of the previous models are only applicable at one field strength. Similarly, neither of the previous models account for hematocrit differences, which *do* affect the resulting ΔR1, as we have now demonstrated in this manuscript and as was actually measured in human lung tissue by Kindvall et al.[23] Therefore, although it is not possible to provide a robust comparison of this model to the previous two models, we are confident that this model brings significant improvements for two main reasons: first, the utility of this model surpasses the previous models simply by the fact that the previous models only apply to a single field strength.[22,23] OE-MRI research occurs at a variety of field strengths, and therefore the model must account for the effect of B0 on each of the relevant variables. This field-strength consideration is an extremely useful feature that will allow data acquired at different field strengths to be compared. Second, one previous model incorrectly combines values from different field strengths into one single model (using $r1_{dHb}$ from Silvennoinnen et al.[24] at 4.7T alongside $r1_{Ox}$ from Pilkinton et al.[46] at 1.5T), which suggests it will be produce slightly incorrect results at any field strength.[22] In summary, we present a new model that is more accurate and considers important factors such as field strength and hematocrit. Most of all, however, our work extends the previous modeling work in significant ways, in particular by incorporating the concept of OEF and introducing an alternative approach to incorporating metabolic rate.

Last, a number of assumptions are necessarily made in the generation of this model, however one may be particularly problematic for some research applications: the assumption from the Krogh tissue model that all capillaries are parallel, unbranched, and equally spaced. While this may be a reasonable assumption in the brain and certain other organs, in others it is a very poor assumption. i.e. the placenta, where OE-MRI has been used successfully.[47] Importantly, this is also a very poor assumption in tumors, which often have severely deranged vasculature, including tortuous and elongated capillaries.[48] This is a major limitation of using the Krogh model to estimate the tissue PO_2 changes, as deviations from the simplistic geometry assumed may cause misinterpretations. For example, complex geometry will affect the ability to estimate R_t, which will then cause errors in the modeled metabolic rate. Fortunately, the modular nature of this model and the supplied code allows researchers to easily substitute more modern tissue oxygen diffusion and consumption models that do account for abnormal vasculature, or any other particular qualities that their tissue of interest may require.

6 | CONCLUSIONS

In conclusion, we have proposed a three-compartment model for estimating the changes in R1 that could be expected in various tissues depending on field strength B0, SO_2, BV, hematocrit, oxygen extraction fraction (OEF), and changes in blood and tissue PO_2. In a demonstration of the model, the resulting ΔR1 are consistent with reported

literature OE-MRI results in a variety of tissues. This model has been designed to be easy for researchers to tailor to their tissue of interest by substituting their preferred model for tissue oxygen diffusion and consumption.

ACKNOWLEDGMENTS

E.B. is supported by funding from the Engineering and Physical Sciences Research Council (EPSRC) and Medical Research Council (MRC) [grant number EP/L016052/1] and the Clarendon Scholarship fund. DB and ES also gratefully acknowledge funding from the EPSRC [grant numbers EP/S021507/1 and EP/L024012/1]. E.B. thanks Richard Sove for helpful discussions about Krogh modelling.

DATA AVAILABILITY STATEMENT

The model has been hosted open-source at [github.com/BulteGroup/TissueR1Model] for other researchers to adopt, adapt and improve.

ORCID

Emma Bluemke https://orcid.org/0000-0001-5970-9100

TWITTER

Emma Bluemke @emmabluemke

REFERENCES

1. Berkowitz BA, Wilson CA. Quantitative mapping of ocular oxygenation using magnetic resonance imaging. *Magn Reson Med*. 1995;33:579-581.
2. Simpson ARH, Dowell NG, Jackson TL, Tofts PS, Hughes EH. Measuring the effect of pars Plana vitrectomy on vitreous oxygenation using magnetic resonance ImagingEffects of PPV on pO2 using MRI. *Investig Ophthalmol Visual Sci*. 2013;54:2028-2034.
3. Muir ER, Zhang Y, Nateras OSE, Peng Q, Duong TQ. Human vitreous: MR imaging of oxygen partial pressure. *Radiology*. 2013;266:905-911.
4. Zaharchuk G, Busse RF, Rosenthal G, Manley GT, Glenn OA, Dillon WP. Noninvasive oxygen partial pressure measurement of human body fluids in vivo using magnetic resonance imaging. *Acad Radiol*. 2006;13:1016-1024.
5. Wang ZJ, Joe BN, Coakley FV, Zaharchuk G, Busse R, Yeh BM. Urinary oxygen tension measurement in humans using magnetic resonance imaging. *Acad Radiol*. 2008;15:1467-1473.
6. Zaharchuk G, Martin AJ, Rosenthal G, Manley GT, Dillon WP. Measurement of cerebrospinal fluid oxygen partial pressure in humans using MRI. *Magn Reson Med*. 2005;54:113-121.
7. Dewhirst MW, Birer SR. Oxygen-enhanced MRI is a major advance in tumor hypoxia imaging. *Cancer Res*. 2016;76:769-772.
8. Little RA, Jamin Y, Boult JKR, et al. Mapping hypoxia in renal carcinoma with oxygen-enhanced MRI: comparison with intrinsic susceptibility MRI and pathology. *Radiology*. 2018;288:739-747.
9. Connor JPB, Robinson SP, Waterton JC. Imaging tumour hypoxia with oxygen-enhanced MRI and BOLD MRI. *Br J Radiol*. 2019;92:20180642.
10. Winter JD, Akens MK, Cheng HLML. Quantitative MRI assessment of VX2 tumour oxygenation changes in response to hyperoxia and hypercapnia. *Phys Med Biol*. 2011;56:1225-1242.
11. Connor JP, Naish JH, Parker GJ, et al. Preliminary study of oxygen-enhanced longitudinal relaxation in MRI: a potential novel biomarker of oxygenation changes in solid tumors. *Int J Radiat Oncol Biol Phys*. 2009;75:1209-1215.
12. Kindvall SSI, Diaz S, Svensson J, Wollmer P, Olsson LE. The change of longitudinal relaxation rate in oxygen enhanced pulmonary MRI depends on age and BMI but not diffusing capacity of carbon monoxide in healthy never-smokers. *pLoS One*. 2017;12:e0177670. doi:10.1371/journal.pone.0177670
13. Morgan AR, Parker GJM, Roberts C, et al. Feasibility assessment of using oxygen-enhanced magnetic resonance imaging for evaluating the effect of pharmacological treatment in COPD. *Eur J Radiol*. 2014;83:2093-2101.
14. Ichiro MK, Bernardo M, Subramanian S, et al. MR assessment of changes of tumor in response to hyperbaric oxygen treatment. *Magn Reson Med*. 2006;56:240-246.
15. Bluemke E, Stride E, Bulte D. A simplified empirical model to estimate oxygen relaxivity at different magnetic fields. *NMR Biomed*. 2021;35:e4625. doi:10.1002/nbm.4625
16. Vatnehol SAS, Hol PK, Bjørnerud A, Amiry-Moghaddam M, Haglerød C, Storås TH. Effect of drinking oxygenated water assessed by in vivo MRI Relaxometry. *J Magn Reson Imaging*. 2020;52:720-728.
17. Yang DM, Arai TJ, Campbell JW, Gerberich JL, Zhou H, Mason RP. Oxygen-sensitive MRI assessment of tumor response to hypoxic gas breathing challenge. *NMR Biomed*. 2019;32:e4101. doi:10.1002/nbm.4101
18. Blockley NP, Jiang L, Gardener AG, Ludman CN, Francis ST, Gowland PA. Field strength dependence of R 1 and R2* relaxivities of human whole blood to prohance, vasovist, and deoxyhemoglobin. *Magn Reson Med*. 2008;60:1313-1320.
19. Bluemke E, Stride E, Bulte D. A general model to calculate the spin-lattice relaxation rate (R1) of blood, accounting for haematocrit, oxygen saturation, oxygen partial pressure, and magnetic field strength under hyperoxic conditions. *J Magn Reson Imaging*. 2021;55:1428-1439.
20. Bhogal AA, Siero JC, Zwanenburg J, Luijten PR, Philippens ME, Hoogduin H. Quantitative T1 mapping under precisely controlled graded hyperoxia at 7T. *J Cereb Blood Flow Metab*. 2017;37:1461-1469.
21. Muir ER, Cardenas DP, Duong TQ. MRI of brain tissue oxygen tension under hyperbaric conditions. *NeuroImage*. 2016;133:498-503.
22. Holliday K. *Oxygen-Enhanced MRI in Cancer*. The University of Manchester; 2013 Accessed August 13, 2021. https://www.research.manchester.ac.uk/portal/files/54548076/FULL_TEXT.PDF
23. Kindvall S. *Pulmonary Imaging with Quantification of T1-Relaxation and Oxygen Enhanced MRI*. Lund University: Faculty of Medicine; 2018 Accessed May 21, 2021. https://lucris.lub.lu.se/ws/portalfiles/portal/54271318/Simon_e_spik_ex.pdf
24. Silvennoinen MJ, Kettunen MI, Kauppinen RA. Effects of hematocrit and oxygen saturation level on blood spin-lattice relaxation. *Magn Reson Med*. 2003;49:568-571.

25. Welter M, Fredrich T, Rinneberg H, Rieger H. Computational model for tumor oxygenation applied to clinical data on breast tumor hemoglobin concentrations suggests vascular dilatation and compression. Secomb TW, ed. *pLoS ONE*. 2016;11:e0161267. doi:10.1371/journal.pone.0161267
26. Rasmussen P, Nielsen J, Overgaard M, et al. Reduced muscle activation during exercise related to brain oxygenation and metabolism in humans: central fatigue *versus* brain oxygenation and metabolism. *J Physiol*. 2010;588:1985-1995.
27. Gjedde A, Johannsen P, Cold GE, Østergaard L. Cerebral metabolic response to low blood flow: possible role of cytochrome oxidase inhibition. *J Cereb Blood Flow Metab.* 2005;25:1183-1196.
28. Rasmussen P, Dawson EA, Nybo L, van Lieshout JJ, Secher NH, Gjedde A. Capillary-oxygenation-level-dependent near-infrared spectrometry in frontal lobe of humans. *J Cereb Blood Flow Metab.* 2007;27:1082-1093.
29. Kety SS. Determinants of tissue oxygen tension. *Fed Proc*. 1957;16:666-671.
30. Goldman D. Theoretical models of microvascular oxygen transport to tissue. *Microcirculation*. 2008;15:795-811.
31. Connor JPB, Jackson A, Buonaccorsi GA, et al. Organ-specific effects of oxygen and carbogen gas inhalation on tissue longitudinal relaxation times. *Magn Reson Med*. 2007; 58:490-496.
32. Li W, Grgac K, Huang A, Yadav N, Qin Q, van Zijl PCM. Quantitative theory for the longitudinal relaxation time of blood water. *Magn Reson Med*. 2016;76:270-281.
33. Less JR, Skalak TC, Sevick EM, Jain RK. Microvascular Architecture in a Mammary Carcinoma: Branching Patterns and Vessel Dimensions.:10.
34. Ivanov KP, Kalinina MK, Levkovich YI. Blood flow velocity in capillaries of brain and muscles and its physiological significance. *Microvasc Res*. 1981;22:143-155.
35. Cho J, Lee J, An H, Goyal MS, Su Y, Wang Y. Cerebral oxygen extraction fraction (OEF): comparison of challenge-free gradient echo QSM+qBOLD (QQ) with 15O PET in healthy adults. *J Cereb Blood Flow Metab*. 2021;41:1658-1668.
36. Leenders KL, Perani D, Lammertsma AA, et al. Cerebral blood flow, blood volume and oxygen utilization: normal values and effect of age. *Brain*. 1990;113:27-47.
37. Qi XL, Burns P, Hong J, Stainsby J, Wright G. Characterizing blood volume fraction (BVF) in a VX2 tumor. *Magn Reson Imaging*. 2008;26:206-214.
38. Nguyen TK. Mass Transfer, Ch 1-6, CHE313. *Chemical and Material Engineering Department, California State Polytechnic University*; 2012:51-60 https://www.cpp.edu/tknguyen/
39. McGuire BJ, Secomb TW. A theoretical model for oxygen transport in skeletal muscle under conditions of high oxygen demand. *J Appl Physiol*. 2001;91:2255-2265.
40. Fry BC, Roy TK, Secomb TW. Capillary recruitment in a theoretical model for blood flow regulation in heterogeneous microvessel networks. *Physiol Rep*. 2013;1:e00050. doi:10.1002/phy2.50
41. Burrell JS, Walker-Samuel S, Baker LC, et al. Exploring ΔR(2) * and ΔR(1) as imaging biomarkers of tumor oxygenation. *J Magn Reson Imaging: JMRI*. 2013;38:429-434.
42. Carinci F, Meyer C, Phys D, et al. Blood volume fraction imaging of the human lung using intravoxel incoherent motion. *J Magn Reson Imaging*. 2015;41:1454-1464.
43. Paech D, Nagel AM, Schultheiss MN, et al. Quantitative dynamic oxygen 17 MRI at 7.0 T for the cerebral oxygen metabolism in glioma. *Radiology*. 2020;295:181-189.
44. Beeman SC, Shui YBB, Perez-Torres CJ, Engelbach JA, Ackerman JJ, Garbow JR. O2 -sensitive MRI distinguishes brain tumor versus radiation necrosis in murine models. *Magn Reson Med*. 2016;75:2442-2447.
45. Tadamura E, Hatabu H, Li W, Prasad PV. Edelman RR. Effect of oxygen inhalation on relaxation times in various tissues. *J Magn Reson Imaging*. 1997;7:220-225.
46. Pilkinton DT, Hiraki T, Detre JA, Greenberg JH, Reddy R. Absolute cerebral blood flow quantification with pulsed arterial spin labeling during hyperoxia corrected with the simultaneous measurement of the longitudinal relaxation time of arterial blood. *Magn Reson Med*. 2012;67:1556-1565.
47. Huen I, Morris DM, Wright C, et al. R1 and R2* changes in the human placenta in response to maternal oxygen challenge. *Magn Reson Med*. 2013;70:1427-1433.
48. Nagy JA, Chang SH, Dvorak AM, Dvorak HF. Why are tumour blood vessels abnormal and why is it important to know? *Br J Cancer*. 2009;100:865-869.

SUPPORTING INFORMATION

Additional supporting information may be found in the online version of the article at the publisher's website.

Figure S1: The (A) total oxygen content (CaO_2), (B) SO_2, and (C) PO_2 along the capillary for OEF ranging from 0.2–0.4

Figure S2: (A) The behavior of the oxygen consumption rate (M) as described by the Michaelis–Menten model (Equation 10) for a range of values chosen for P_{crit} (0.5-4 mmHg). (B) The behavior of PO_2 into the tissue radius as described by the Krogh-Erlang solution (Equation 9), is shown for a range of M_0 to illustrate the effect of different rates of M_0 on PO_2 (with constant $P_{cap} = 90$ mmHg).

Figure S3: (A) An illustration of a 3D voxel of tissue with capillaries as cylinders that are parallel, unbranched, and equally spaced throughout the voxel. (B) The inverse relationship between blood volume and the Krogh Radius R_t resulting from following this method

Figure S4: Example 3D surface plots (shown from two viewing angles) of the PO_2 into the tissue radius and along the capillary, on (A) air and (B) oxygen breathing, assuming a post-oxygen arterial PO_2 change from 90-200mHg.

Figure S5: A schematic of Step 4, where the ΔR1 from each compartment is weighted by the volume fraction of each compartment within the voxel. The final $\Delta R1_{voxel}$ is the sum of the weighted components

Figure S6: Simulated data showing the resulting (A) mean tissue PO_2, (B) minimum tissue PO_2, and (C) maximum oxygen consumption rate resulting from all combinations of the ranges of blood volume and OEF used. (D) The blood

volume vs. mean tissue PO_2 is shown for just OEF = 0.4, to show the subtle curve not visible in plots A-B due to the scale of the y-axis. All plots use $PaO_2 = 90$ mmHg

Table S1: The OE-MRI response in different tissue types identified by various studies

How to cite this article: Bluemke E, Stride E, Bulte DP. Modeling the Effect of Hyperoxia on the Spin–Lattice Relaxation Rate R1 of Tissues. *Magn Reson Med*. 2022;88:1867-1885. doi: 10.1002/mrm.29315